An adaptive moving mesh method with application to non-stationary hypersonic flows in the atmosphere

S V Utyuzhnikov[1]* and **D V Rudenko**[2]
[1]School of Mechanical Aerospace and Civil Engineering, University of Manchester, Manchester, UK
[2]Department of Computational Mathematics, Moscow Institute of Physics & Technology, Dolgoprudny, Russia

The manuscript was received on 21 July 2007 and was accepted after revision for publication on 8 November 2007.

DOI: 10.1243/09544100JAERO261

Abstract: A numerical algorithm based on a shock-capturing scheme on adaptive moving meshes is described. Three-dimensional dynamical adaptive meshes are generated as the result of solving a variational problem. The governing equations are solved in a moving coordinate system therefore the method does not require any interpolation of the solution from one mesh onto another one. The developed algorithm can efficiently be used for the simulation of non-stationary supersonic flows in the atmosphere. As an example, it is applied to the study of the Tunguska meteorite hypersonic impact. For the first time this problem is modelled from the entrance moment up to the interaction with the Earth atmosphere in a three-dimensional formulation. A reasonable correspondence with the data of the observations is obtained. The implementation of the developed numerical algorithm reduces the computational time by the factor of four.

Keywords: adaptive mesh, interpolation-free method, shock-capturing scheme, grid generation, hypersonic impact, atmosphere, Tunguska meteorite

1 INTRODUCTION

Numerical simulation of flows with strong shock waves and other possible high gradients of the solution requires the use of fine meshes for an appropriate resolution. Simple algorithms based on uniform meshes might be time-consuming because of a high number of unknown grid variables. The situation is aggravated for multi-dimensional problems. A standard way to an efficient resolution is related to the implementation of meshes adaptive to the areas of the high gradients (see e.g. [**1**]). Meanwhile, for non-stationary problems such algorithms become much more complicated because, shock waves move in space and interact with each other. One possible way (see e.g. [**2**–**6**]) to overcome this problem is based on a mesh reconstruction each time the solution 'substantially' changes. The realization of this approach requires interpolation of the solution from one mesh onto another mesh. This procedure might introduce an additional error and be time-consuming. An alternative strategy is based on interpolation-free methods (see e.g. [**7**–**13**]). Most of these works are related to one- and two-dimensional problems. In the current paper, a interpolation-free algorithm [**14**, **15**] based on the use of a moving coordinate system is developed for modelling the hypersonic non-stationary motion of bodies in the Earth atmosphere.

The developed algorithm is applied to the study of the Tunguska meteorite impact. This event happened in 1908 in Siberia, 100 years ago. Up to now it arises a high interest from many researches (see e.g. [**16**–**25**]). In particular, the nature of the Tunguska meteorite is the subject of intensive discussions [**16**, **18**, **20**, **22**, **24**]. The Tunguska impact caused vast destruction of the forest in the area of about 10^8 m^2 and was accompanied by explosion-like phenomena. The data of the observation were limited by the fallen trees and description of some witnesses.

Corresponding author: School of Mechanical Aerospace and Civil Engineering, University of Manchester, George Begg Building, Sackville Street, PO Box 88, Manchester M60 1QD, UK. email: s.utyuzhnikov@manchester.ac.uk

Thus, mathematically the problem on the Tunguska meteorite study can be considered as a typical inverse problem. Many papers have been related to the investigation of this problem including numerical simulation of different scenarios of the impact. In reference [**17**], the problem was approximately solved in local one-dimensional directions. Meanwhile, there have not been yet any publications based on a three-dimensional simulation of the entire process from the entrance and up to the interaction with the Earth surface. In the current paper, the entire process is studied in a non-stationary three-dimensional formulation and simulated in a unified computation. The computational results on the interaction between the blow shock wave and the Earth surface are compared against the observation data on the fallen forest.

2 GOVERNING EQUATIONS

First, let the Euler equations for a compressible gas in the Cartesian coordinate system $\{y^i, t\}$, $i = 1, 2, 3$ be written as follows

$$U_{\mathrm{t}} + \sum_1^3 F^i_{y^i} = Q \tag{1}$$

where $U = (\rho, \rho u_1, \rho u_2, \rho u_3, E)^{\mathrm{T}}$, $F^i = (\rho u_i, \rho u_1 u_i + p\delta_{1i}, \rho u_2 u_i + p\delta_{2i}, \rho u_3 u_i + p\delta_{3i}, (E+p)u_i)^{\mathrm{T}}$, $Q = (0, \rho g_1, \rho g_2, \rho g_3, \rho \boldsymbol{g}\cdot\boldsymbol{u}, 0)^{\mathrm{T}}$, $E = \rho(\epsilon + 0.5\boldsymbol{u}\cdot\boldsymbol{u})$, $p = p(\rho, \epsilon)$, δ_{ij} is the Kronecker symbol.

In equation (1), ρ is the density; $\boldsymbol{u} = (u_1, u_2, u_3)^{\mathrm{T}}$ is the velocity; ϵ is the specific internal energy, E is the total internal energy, p is the pressure, $\boldsymbol{g} = (g_1, g_2, g_3)^{\mathrm{T}}$ is the gravity vector.

To introduce a local moving coordinate system, let the set of equations (1) in an arbitrary non-singular curvilinear coordinate system (τ, ξ): $\xi = \xi(t, \boldsymbol{y})$, $\tau = t$ preserving the rigorous conservative form be rewritten as follows

$$\frac{\partial}{\partial\tau}(\hat{U}) + \sum_{i=1}^3 \frac{\partial}{\partial\xi^i}(\hat{F}_i) = \hat{Q} \tag{2}$$

here

$$\hat{U} = \frac{U}{J}, \quad \hat{F}_i = \hat{\xi}^i_t U + \sum_1^3 \hat{\xi}^i_{y^j} F^j, \quad \hat{Q} = \frac{Q}{J}$$

$$\hat{\xi}^i_t = \frac{\xi^i_t}{J}, \quad \hat{\xi}^i_{y^j} = \frac{\xi^i_{y^j}}{J}, \quad J = \det\|\xi^i_{y^j}\| \quad (i, j = 1, 2, 3)$$

In numerical solution of equation (2) it is natural to demand that a uniform flow $U = \mathrm{const}$ must be a partial solution of this set of equations for any non-singular coordinate system if $Q = 0$. This requirement results in the following set of equations called the geometric conservation laws [**7**]

$$\frac{\partial}{\partial\tau}\left(\frac{1}{J}\right) + \sum_1^3 \frac{\partial}{\partial\xi^j}(\hat{\xi}^j_t) = 0,$$

$$\frac{\partial}{\partial\xi^j}(\hat{\xi}^j_{y^i}) = 0 (i = 1, 2, 3) \tag{3}$$

Conditions (3) imply that the constant solution of equation (2) is invariant with respect to the coordinate transformations. To satisfy these requirements the Jacobian of the transformation to the new coordinates is to be determined immediately from the conservation laws (3) rather than by the formula $J = \det\|\xi^i_{y^j}\|$ [**14**].

3 FINITE-DIFFERENCE APPROXIMATION

To approximate the governing equations, the UNO-type (uniformly non-oscillatory) scheme [**26**, **27**] is used. This scheme is of the second-order in both space and time variables. The approximation of set (2) is realized via the 'predictor-corrector' algorithm.

A rectangular uniform grid ξ^l_{ijk} can be used in the new variable ξ

$$\xi^l_{ijk} = ih_1, \xi^2_{ijk} = jh_2, \xi^3_{ijk} = jh_3$$

$$i = 0, \ldots, N_1, \quad j = 0, \ldots, N_2, \quad k = 0, \ldots, N_3$$

where $h_l = 1/N_l$, $l = 1, 2, 3$, and N_l is the number of computational cells along an lth direction.

The rectangular uniform grid ξ^l_{ijk} maps onto a curvilinear grid: $y^l_{ijk} = y^l_{ijk}(\xi^1_{ijk}, \xi^2_{ijk}, \xi^3_{ijk}, \tau)$, $(l = 1, 2, 3)$ in the physical domain.

The finite-difference approximation of the set (2) on the uniform rectangular grid ξ^l_{ijk} reads as follows

$$V_{ijk}\frac{\hat{U}^{n+1}_{i,j,k} - \hat{U}^n_{i,j,k}}{\tau} + (\hat{F}^1 S_{\xi^1})_{i+1/2,j,k} - (\hat{F}^1 S_{\xi^1})_{i-1/2,j,k}$$
$$+ (\hat{F}^2 S_{\xi^2})_{i,j+1/2,k} - (\hat{F}^2 S_{\xi^2})_{i,j-1/2,k} + (\hat{F}^3 S_{\xi^3})_{i,j,k+1/2}$$
$$- (\hat{F}^3 S_{\xi^3})_{i,j,k-1/2} = \hat{Q}_{i,j,k}$$

where $V_{i,j,k}$ is the volume of a computational cell (i, j, k), $(S_{\xi^1})_{i\pm1/2,j,k} = h_2 h_3$, $(S_{\xi^2})_{i,j\pm1/2,k} = h_1 h_3$, and $(S_{\xi^3})_{i,j,k\pm1/2} = h_1 h_2$ are the areas of the corresponding faces of the cell, and $\Delta\tau$ is the time step. The function $\hat{U}^n_{ijk}$ sought and the source terms $\hat{Q}_{ijk}$ are calculated at the centres of computational cells, and fluxes $\hat{F}^1_{i\pm1/2,j,k}$, $\hat{F}^2_{i,j\pm1/2,k}$, $\hat{F}^3_{i,j,k\pm1/2}$, at the centres of the corresponding faces.

The time approximation is organized in the 'predictor–corrector' form. To simplify formulas the case where the solution varies only along one coordinate is considered

$$\tilde{U}_{ijk}^{n+1} = U_{ijk}^{n} - \frac{\Delta\tau}{h_1}(\hat{F}^1(U_{i+1/2,j,k}^{-}) - \hat{F}^1(U_{i-1/2,j,k}^{+}))$$

where $U_{i+1/2,j,k}^{-} = U_{ijk}^{n} + 0.5\delta U_{ijk}$, $U_{i-1/2,j,k}^{+} = U_{ijk}^{n} - 0.5\delta U_{ijk}$, and δU_{ijk} is the limited variation first introduced by Kolgan [**28**]

$$\delta U_{ijk} = \text{minmod}\frac{(U_{i+1,j,k} - U_{i,j,k}, U_{i,j,k} - U_{i-1,j,k})}{h_1}$$

$$\text{minmod}(x, y) \stackrel{\text{def}}{=} \begin{cases} \min(|x|, |y|) & \text{if } x \cdot y \geqslant 0 \\ 0 & \text{if } x \cdot y < 0 \end{cases}$$

Then, the ultimate solution is obtained as follows

$$U_{i+1/2,j,k}^{n+1/2,-} = 0.5(\tilde{U}_{i,j,k}^{n+1} + 0.5\delta U_{ijk} + U_{i+1/2}^{-})$$

$$U_{i-1/2,j,k}^{n+1/2,+} = 0.5(\tilde{U}_{ijk}^{n+1} - 0.5\delta U_{ijk} + U_{i-1/2,j,k}^{+})$$

$$U_{ijk}^{n+1} = U_{ijk}^{n} - \frac{\Delta\tau}{h_1}\left(\hat{F}^1\left(U_{i+1/2,j,k}^{n+1/2,-}\right) - \hat{F}^1\left(U_{i-1/2,j,k}^{n+1/2,+}\right)\right)$$

Thus, one has an opportunity to solve the governing equations on a rectangular uniform mesh and separate this procedure from the grid generation. As a result, one has two domains: the computational and the physical. In the computational domain the mesh is uniform and fixed, while in the physical domain one has a dynamical curvilinear grid. The extension of the approach to the Navier–Stokes equations can be done without any substantial modifications.

4 GRID GENERATION

The new variables $\xi^i = \xi^i(y, t)$, $(i = 1, 2, 3)$ should be chosen in such a way that the solution $U = U(\xi^1, \xi^3, \xi^3, \tau)$ does not have severe gradients. In turn, the inverse transform from the new variables to the original Cartesian coordinates should also be smooth to avoid any singularities. Hence, the adaptive grid should be smooth and orthogonal enough. It is clear that it is possible to fully satisfy all these requirements only in trivial cases. Thus, the challenge is to find an appropriate transformation of the coordinates to provide a trade-off between the desired properties.

To solve the described above multi-objective optimization problem, the variational approach [**29**] developed for a stationary mesh generation has been generalized to non-stationary problems. According to this approach, an aggregate function is constructed as a weighted-sum of the functionals corresponding to the objective functions responsible for the adaptivity, smoothness and orthogonality.

The adaptivity functional controls the concentration of grid nodes in the regions where the gradients of the solution are severe. It is represented by the following integral

$$I_{\text{w}} = \int\int\int W^2 g^{1/2} \text{d}y^1 \text{d}y^2 \text{d}y^3 = \int\int\int W^2 g \, \text{d}\xi^1 \text{d}\xi^2 \text{d}\xi^3 \tag{4}$$

where g_{ij} is the metrical tensor: $g_{ij} = \boldsymbol{r}_{\xi^i} \cdot \boldsymbol{r}_{\xi^j}$, $g = \det\|g_{ij}\|$ $(i, j = 1, 2, 3)$; W is a weight function. It is natural to choose the weight function such that it is positive and proportional to the gradient of the solution in the new variables. The following weight function was used in the calculations

$$W^2 = \sqrt{1 + \alpha|\nabla_\xi f|^2} \tag{5}$$

here f is an unknown function to be determined from the solution; it may be the pressure, density, temperature, etc., or a weighted sum of these, depending on a particular problem under consideration.

The minimization of the functional I_{w} causes the redistribution of the grid nodes from the regions with lesser values of the weight function to those with its greater values. If the weight function is constant in the computational domain, the mesh remains uniform. In computations the grid remained uniform if the variations of the weight function were less than 1 per cent of its average value in the region. Thus, by using the parameter α the regions with considerable adaptation can be confined to those where the gradients of the solution are greater than a certain value. For this purpose, the parameter α should be the following: $\alpha = \Lambda(|\nabla_\xi f|)^2$, where $0.1 < \Lambda < 10$.

In turn, the grid smoothness and orthogonality are described by the diagonal and non-diagonal elements of the metric tensor, respectively. The corresponding functionals have the following form

$$I_{\text{s}} = \int\int\sum_{i=1}^{3} g^{ii} \text{d}y^1 \, \text{d}y^2 \, \text{d}y^3 = \int\int\int\left(\sum_{i=1}^{3}(g_{jj}g_{kk} - g_{jk}^2)g^{-0.5}\right)\text{d}\xi^1 \, \text{d}\xi^2 \, \text{d}\xi^3 \tag{6}$$

$$I_{\text{o}} = \int\int\int g^{3/2}\sum_{i=1}^{3}(g^{jk})^2 \text{d}y^1 \, \text{d}y^2 \, \text{d}y^3 = \int\int\int\sum_{i=1}^{3}(g_{ij}g_{ik} - g_{ii}g_{jk})\text{d}\xi^1 \, \text{d}\xi^2 \, \text{d}\xi^3 \tag{7}$$

Here, the indexes (*i, j, k*) are varied in the cyclic order, thereby the value of the index *i* fully determines the values of the other indexes.

Thus, the construction of the mesh is reduced to the minimization of the following aggregate cost function

$$I \equiv \int\int\int F \mathrm{d}\xi^1\, \mathrm{d}\xi^2\, \mathrm{d}\xi^3 = I_\mathrm{s} + \lambda_\mathrm{o} I_\mathrm{o} + \lambda_\mathrm{w} I_\mathrm{w} \tag{8}$$

The minimum of the cost function I can be found by the Euler–Lagrange method. As a result, one can arrive at the following set

$$\sum_1^3 \frac{\partial}{\partial \xi^j} \frac{\partial F}{\partial (y^i)_{\xi^j}} - \frac{F}{\partial y^i} = 0, \quad (i = 1, 2, 3)$$

After some transforms, one can obtain the set of equations in the curvilinear coordinates with regard to the metric coefficients

$$\sum_1^3 A_{jj} \boldsymbol{r}_{\xi^j \xi^j} = \boldsymbol{b} \tag{9}$$

where

$$\boldsymbol{b} = F_\mathrm{W} \nabla W - \left(\sum_{j=1}^3 \sum_{\substack{k=1 \\ k\neq j}}^3 A_{jk} \boldsymbol{r}_{\xi^j \xi^k} + \sum_{j=1}^3 \sum_{k=1}^3 A'_{jk} W_{\xi^j} \boldsymbol{r}_{\xi^k} + \sum_{j=1}^3 \sum_{k=1}^3 \sum_{m=1}^3 \sum_{n=1}^3 A_{jkmn} (\boldsymbol{r}_{\xi^j \xi^m} \cdot \boldsymbol{r}_{\xi^n}) \boldsymbol{r}_{\xi^k} \right)$$

$$A_{jk} = \frac{\partial F}{\partial g_{jk}} + \frac{\partial F}{\partial g_{kj}}, \quad A'_{jk} = \frac{\partial F_W}{\partial g_{jk}} + \frac{\partial F_W}{\partial g_{kj}}$$

$$A_{jkmn} = \frac{\partial A_{jk}}{\partial g_{mn}} + \frac{\partial A_{jk}}{\partial g_{nm}}, \quad F_\mathrm{W} = \frac{\partial F}{\partial W}$$

It is possible then to obtain the equations for the grid nodes velocities by the differentiation of the Euler–Lagrange equations

$$\sum_{j=1}^3 \sum_{k=1}^3 \frac{\partial}{\partial \xi^j} (A_{jk} \dot{\boldsymbol{r}}_{\xi^k}) = \nabla_y \dot{F} - \sum_{j=1}^3 \sum_{k=1}^3 \frac{\partial}{\partial \xi^j} (\dot{A}_{jk} \boldsymbol{r}_{\xi^k})$$

$$F = F_\mathrm{s} + \lambda_\mathrm{o} F_\mathrm{o} + \lambda_\mathrm{w} F_\mathrm{w}$$

The grid generation set (9) is solved in the cube [0, 1] × [0, 1] × [0, 1] with the following boundary conditions. A fixed node distribution is used on one of the boundaries. It is taken from the previous time layer and corrected according to the condition of orthogonality between a boundary and the appropriate coordinate lines. On the other boundaries the orthogonality condition results in the boundary conditions: $\boldsymbol{r}_{\xi^i} - \boldsymbol{n}_i (\boldsymbol{r}_{\xi^i} \cdot \boldsymbol{n}_i) = 0$, where n_i is the normal to an *i*th boundary. The grid is up-graded each time after the number of time steps depending on the problem to be solved.

The set of Lagrange–Euler equations (9) is elliptic. Upon approximation one can obtain a set of algebraic equations

$$L^{(h)} \boldsymbol{r} = \boldsymbol{b}^{(h)} \tag{10}$$

where $\boldsymbol{b}^{(h)}$ is the projection of the right-hand side vector $\boldsymbol{b}$ in equation (9) onto the appropriate discrete space.

To speed-up the solution of equation (10) complemented by the appropriate boundary conditions, a preconditioning Laplace-based operator B is introduced

$$B\boldsymbol{r}^{n+1} = B\boldsymbol{r}^n - \frac{1}{\lambda_\mathrm{max}} [L^{(h)} \boldsymbol{r}^n - \boldsymbol{b}^{(h)}] \tag{11}$$

where

$$B\boldsymbol{r}^n = \sum_1^3 \frac{\theta_\mathrm{p}}{\lambda_\mathrm{p}} L_\mathrm{pp} \boldsymbol{r}^{(n)} \tag{12}$$

In equation (12), θ_p are the parameters from the interval (0, 1] introduced to make the spectra of the operators B and L/λ_max match each other, L_pp is a one-dimensional difference Laplace operator with respect to a coordinate ξ_p, λ_p is the maximal eigenvalue of L_pp, λ_max is maximal eigenvalue of L evaluated by

$$\lambda_\mathrm{max} = \max_{i,j,k} \left\{ \sum_{i_0=-1}^1 \sum_{j_0=-1}^1 \sum_{k_0=-1}^1 |a_{i+i_0, j+j_0, k+k_0}| \right\}$$

and $a_{i,j,k}$ are the coefficients of the operator $L^{(h)}$ at the node *i,j,k*.

The preconditioning operator B can easily be inverted via the fast Fourier transform along two directions and the Gauss algorithm along the last one. The convergence of the algorithm is sufficiently high. Usually, it requires five to ten iterations to generate a grid. The time required to reconstruct the grid is three to four times smaller than that required for the solution of the main set.

5 TUNGUSKA METEORITE IMPACT PROBLEM

The developed approach is applied to the study of the Tunguska meteorite hypersonic impact into the Earth

atmosphere. This consideration can also be related to the general problem of cometary-asteroid hazard [**24**]. In this analysis the hypothesis of the meteorite nature of the Tunguska object is followed [**24**]. Although a detailed discussion on this question is beyond the scope of the current paper, it is to be noted that the meteorite hypothesis is earnestly supported by the observation data [**23**]. Indeed, in spite of vast efforts of many expeditions to the area of the impact, there have not been found any solid debris of the Tunguska object.

The penetration of meteorites into a dense atmosphere is accompanied by its progressive destruction because of the hypersonic velocity of the meteorite and, hence, the vast pressure behind the blow shock. The aerodynamic loads leads to a sharply accelerated disintegration of the meteorite into smaller and smaller debris which retain approximately the same total volume [**30**]. Because the radius of each piece sharply reduces, the heat transfer suddenly increases. Thus, this process is accompanied by a rapid ablation mechanism. As a result, the whole body is converted into vapour and the kinetic energy of the meteorite is released into the atmosphere. For this process happens almost instantaneously (in comparison to the time of the entire process), it is sometime called the 'explosion-in-flight' [**17**].

On the basis of the consideration given above, the following model of the process [**31**] was used. The meteorite suddenly becomes a gas object at some point of its trajectory. Nevertheless, at the initial time moment, it retains its volume and velocity. The further evolution of this gas object in the atmosphere is modelled numerically. The trajectory

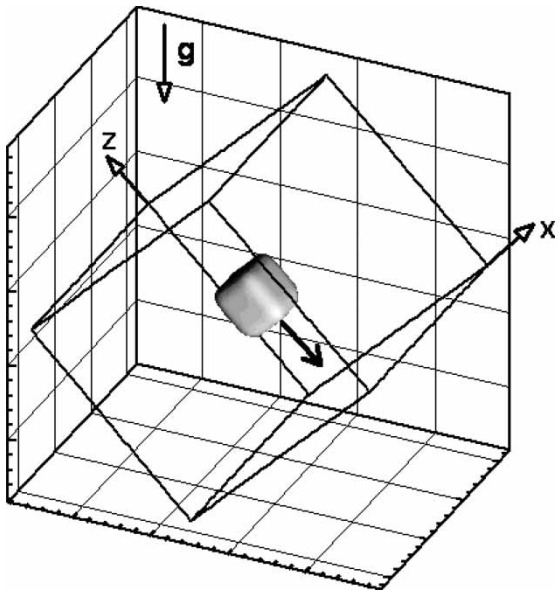

Fig. 1 Coordinate system

point of the sudden conversation is evaluated from Grigoryan's solution [**30**]. It is to be noted that this solution is quite close to the solution by Hills and Goda [**32**] obtained by another way [**24**]. The model described above was earlier used for the modelling of the Shoemaker–Levy Comet impact with Jupiter in reference [**33**].

Thus, one can arrive at the initial statement of the gas dynamic problem. At the initial time moment a gas in some volume V has the following parameters: $m_g = m_0$, $\rho_g = \rho_0$, $V_g = V_\infty$, $P_g = \rho(h)V_\infty^2$ where m_g, ρ_g, V_g, P_g are the mass, density, velocity, and static

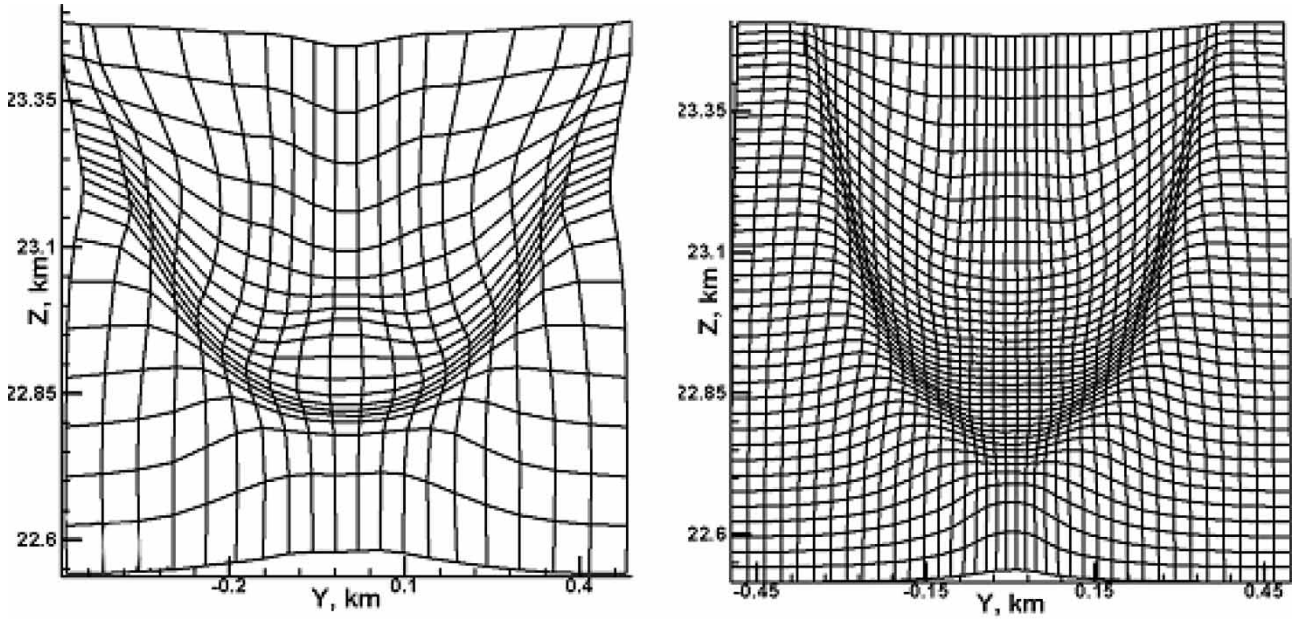

Fig. 2 Adaptive meshes with 20 and 40 nodes in each direction, $t = 0.3$ s

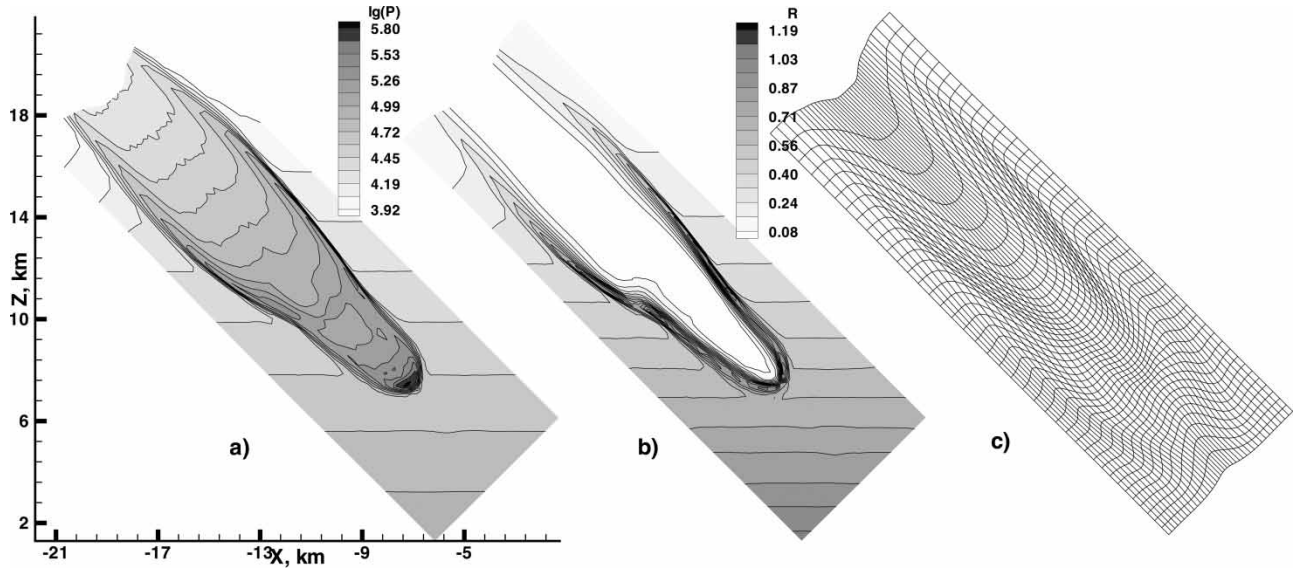

Fig. 3 Contour plots of pressure logarithm and density, computational grid. Section view in plane $Y = 0$ m; $t = 1.7$ s. (a) lg(P); (b) ρ kg/m^3; (c) computational grid

pressure, respectively; m_0, ρ_0, V_∞ are the mass, density, and entrance velocity of the meteorite; $\rho(h)$ is the density of the atmosphere gas at the height of the 'explosion'.

At the current paper, the parameters of the Tunguska meteorite are set the following: $m_0 = 216$ t, $\rho_0 = 10^3$ kg/m^3 (ice body), the characteristic size of a body is $L = 60$ m, $V_\infty = 2 \times 10^4$ m/s. It is supposed

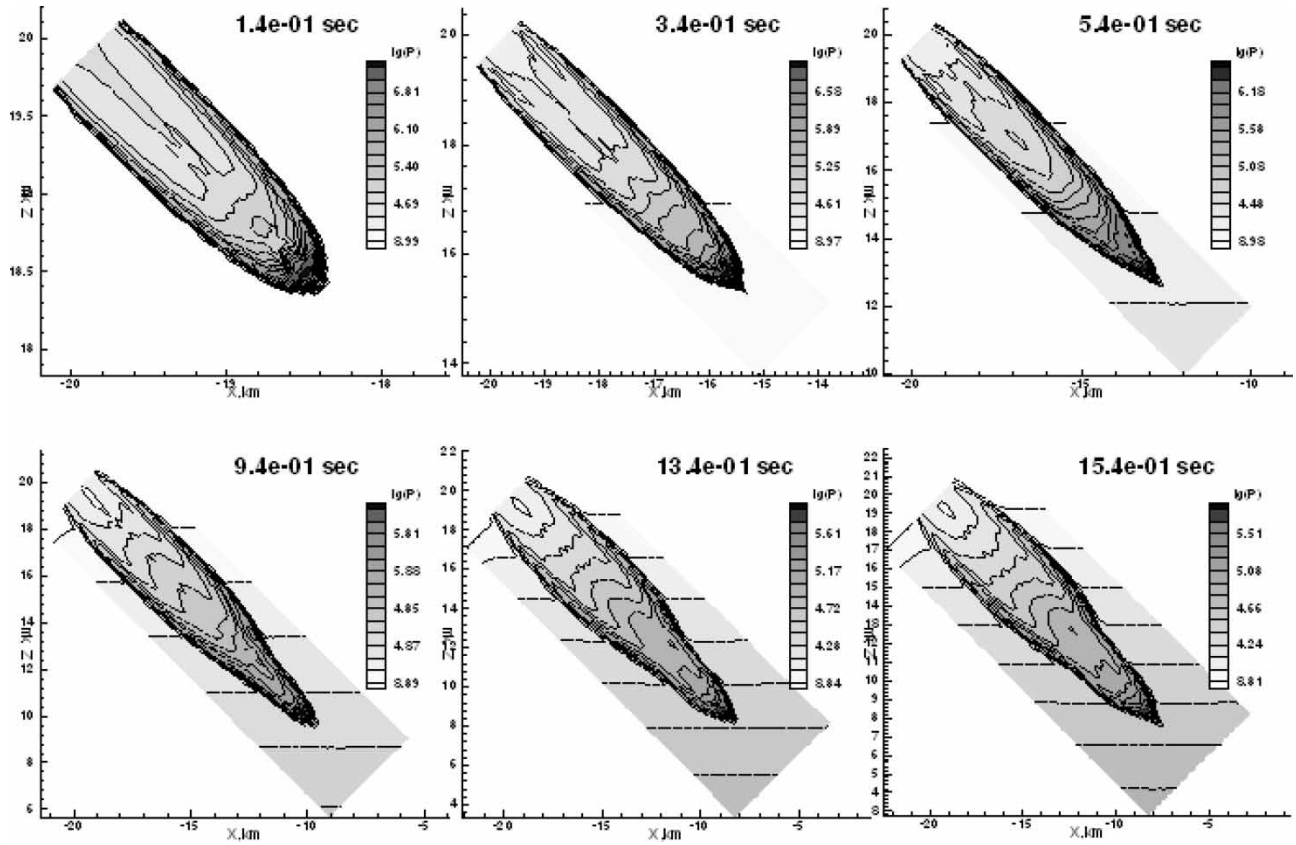

Fig. 4 Evolution of the bow shock wave

that the meteorite enters the atmosphere at the angle of $\Theta = 45^\circ$. These data match 'average' parameters accepted for the Tunguska meteorite [**24**]. Under the chosen parameters, the ratio between the internal energy and the kinetic energy of the meteorite is equal to 4×10^{-4}. Grigorian's semi-analytical solution [**30**] is obtained for an exponential atmosphere $\rho(z) = \rho_0 \exp^{-z/H}$. If $H = 7 \times 10^3$ m, then it gives the following evaluation of the 'explosion' height h: $h = 2.1 \times 10^4$ m.

The gas in the volume and in the atmosphere is considered as an inviscid gas with the state equation of the real air. The meteorite substance is marked by a 'passive' mixture. The weighted-sum-of-gray-gases model (see e.g. [**34**]), is used to take into account the radiation.

The hypersonic of a gas cloud in the atmosphere is accompanied by the formation of the main blow shock and a number of internal shocks and contact discontinuities [**33**]. The entire process is considered starting from the decay of the initial data and up to the interaction of both the shock and gas cloud with the Earth surface.

6 RESULTS OF NUMERICAL SIMULATION

In the numerical study of the problem, the computational domain was first oriented along the direction of the body entrance. As soon as the shock wave reached the Earth surface, the computational area deformed in such a way that the lower boundary of the physical computational domain was parallel to the Earth surface.

At the beginning, the coordinate system was oriented in space in such a way that the axis Z was parallel to the entrance direction and the gravity force vector was in the plane XZ, as shown in Fig. 1. The initial computational domain was a cube with the side of 300 m. The computational domain moved along the axis Z expanding in the space in such a way that the main perturbed flow (apart from the far tail) was captured. Thus, the lower side initially moved towards the Earth surface with the velocity 2×10^4 m/s, while the upper side had the velocity 1.8×10^4 m/s. The lateral sides expanded with the velocity 1.2×10^3 m/s.

In computations, the following function f in equation (5) is used

$$f = 0.5\left(\log\left(\frac{p}{p_0}\right) + \log\left(\frac{\rho}{\rho_0}\right)\right)$$

where the values with '0' are the appropriate typical values in the computational domain. This choice of the function f is justified by the adaptation requirements in both the blow shock area with high pressure and density gradients and the tail area with the high gradients of the density.

The computations were done on different adaptive and uniform meshes. The comparison between the results showed that 40 nodes in each direction were enough to be close to the solution obtained on a uniform mesh of about 10^6 nodes and greater. The main effects can even be captured on a adaptive mesh having only 20 nodes in each direction. The shown

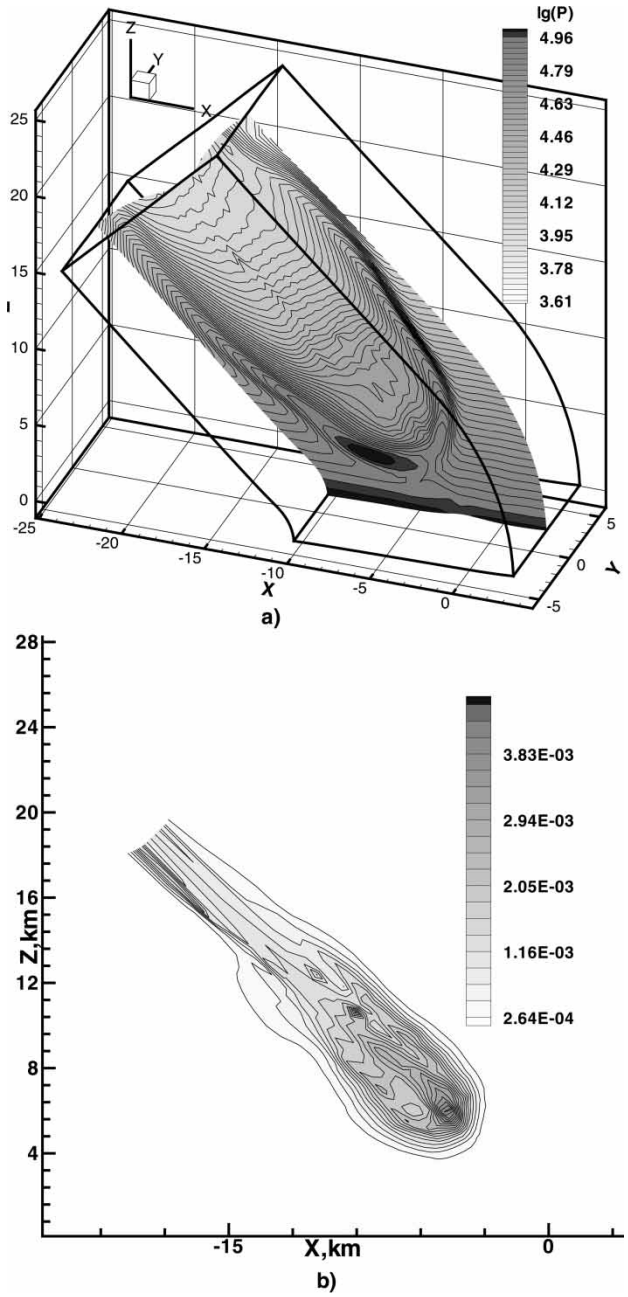

Fig. 5 Contour plots of pressure logarithm and cosmic body substance density. Section view in plane $Y = 0$ m; $t = 8.5$ s. (a) lg(P); (b) ρ_a kg/m^3

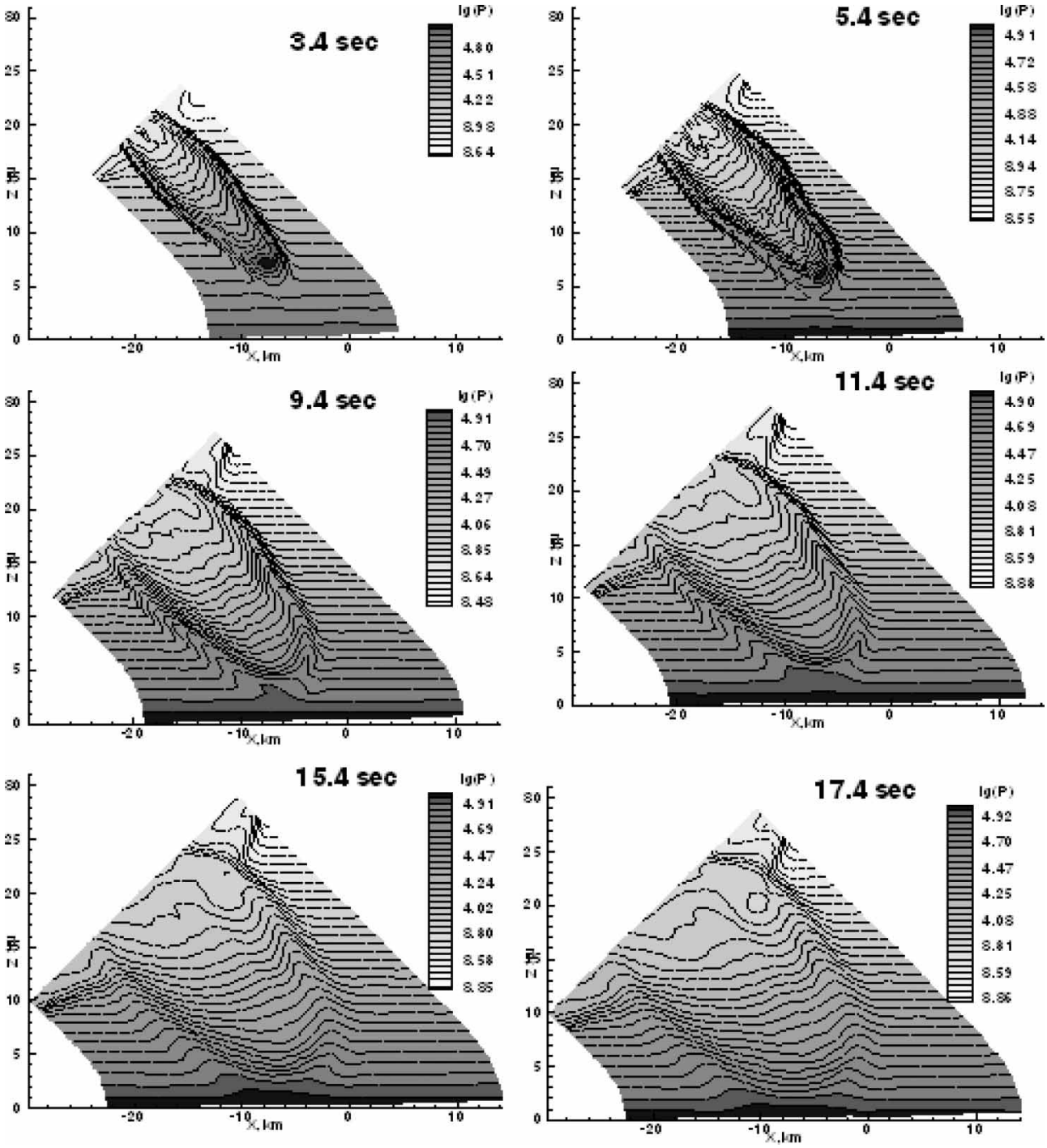

Fig. 6 Long-term evolution of the bow shock wave

further results were obtained on the adaptive grid having 40 nodes in each direction. The computational time was about 3.4 times less against the appropriate result on a uniform mesh. The grid reconstruction was done an each odd time step. It increased the computational time by 20 per cent against the case without adaptation.

The general description of the entire process is the following. By 0.12 s, the meteorite substance forms a bowl-like layer with the typical size of 200 m. The layer is convectively unstable, and, therefore, this leads to the depression of the layer along the direction of the maximal pressure. The meteorite matter forms a torus-like shape. It is worth noting that this phenomenon was earlier observed for the Shoemaker–Levy comet problem [**33**]. Further, the penetration channel of 30 m is filled by a low-density gas and the meteorite matter is fragmented. To

resolve this effect, the typical mesh size must be less than the typical size of the channel. Therefore, it requires either a very fine uniform mesh or an adaptive mesh. It is to be noted that even the 20-node mesh was enough to capture this effect in the case of an adaptive mesh. Meanwhile, the 40-node mesh without adaptation does not allow the resolution of the effect of the meteorite disintegration and provides very different qualitative results.

By 0.3 s, the bow shock wave reaches the height of 1.6×10^4 m, the wave front velocity equals 1.9×10^4 m/s and the characteristic size of the domain is 600 m. By that time the main meteorite cloud is fragmented into several parts and the flow loses the axial symmetry. Adaptive computational meshes with 20 and 40 nodes in each direction are shown in Fig. 2. The degree of the grid adaptivity can be represented by the parameter $k_a = V_{un}/V_{min}$. Here, V_{un} is the cell volume without adaptivity and V_{min} is the minimal cell volume. For the grid shown in Fig. 2 the values of these parameters are 6.3 and 6.2, respectively.

At 1.8 s (Fig. 3) the shock wave, having the maximal pressure $P_{max} = 6.6 \times 10^5$ Pa and the velocity 3.5×10^3 m/s, reaches the level of about 7×10^3 m. Rarefied hot gas flow behind the front of the shock wave has the following parameters: the gas velocity is $7 \times 10^3 - 9 \times 10^3$ m/s, density is 0.3–0.4 kg/m^3, temperature is 7000–8000 K.

After 2 s the bottom of the physical computational domain starts its turn to be parallel to the Earth surface, and it is reached by 3 s. At this time, the shock wave propagation velocity is equaled to 10^3 m/s, while $P_{max} = 8.7 \times 10^5$ Pa. The evolution of the bow shock wave in both space and time is shown in Fig. 4.

It is also interesting to analyse the long-term dynamics of the shock wave and the tail. By the time moment of 8.5 s, the shock wave reaches the level of 2.7×10^3 m, as shown in Fig. 5. It becomes weak and propagates with the velocity 800 m/s. The excessive pressure behind the shock is 0.3 atm. By 9 s, some hot gas in the tail stops and starts to rise up in the atmosphere due to the buoyancy force. The rising flow mainly propagates in the hot tail area. It is important to note that this flow entraps the meteorite substance and prevents it from reaching the Earth. The long-term evolution of the bow shock wave is shown in Fig. 6. By 38 s, the maximal concentration of the meteorite matter is observed on the level of 1.5×10^4 m, in the Earth stratosphere. At the height of 5×10^3 m, the meteorite matter density is less than 4×10^{-3} kg/m^3. Meanwhile, meteorite substance below 3×10^3 m is not observed. Thus, the meteorite matter does not reach the Earth surface, though the shock wave generated by the meteorite significantly affects the Earth surface. This result may explain the failure of all expeditions

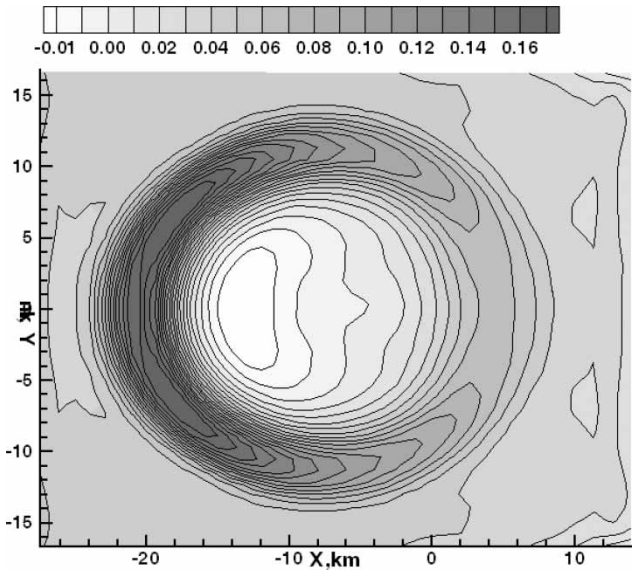

Fig. 7 Distribution of the dynamical pressure on the Earth surface, $t = 38$ s

to find any Tunguska meteorite substance in the area of the impact.

By 12 s, the bow shock reaches the Earth surface. Then, the shock wave with $P_{max} = 1.1 \times 10^5$ Pa spreads over the Earth surface with the velocity of about 6×10^2 m/s along the entrance direction and the velocity of 10^3 m/s along the opposite direction. Then, by 38 s, the maximal velocity drastically drops to 28 m/s.

To consider the interaction of the shock wave with the surface covered by a forest (as happened with the Tunguska meteorite), one should take into

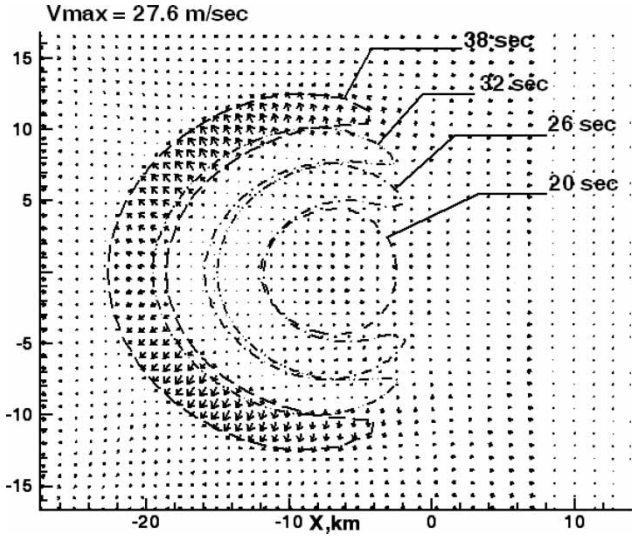

Fig. 8 Distribution of the dynamical pressure greater than 0.1 atm at different time moments

account the dynamic pressure in the flow behind the shock. It is the main characteristics determining the forest flattening. According to reference [**21**] the value of the dynamical pressure 8×10^2 Pa corresponds to the fall of about 5 per cent of all the trees. Then, one obtains that the forest can strongly be damaged in the region with the characteristic size of about 2×10^4 m, as shown in Fig. 7. The areas of the exceed dynamic pressure greater than 0.1 atm are represented in Fig. 8. It is to be noted that this result is in a good correspondence with the observation data for the Tunguska meteorite [**16**, **21**, **24**].

Thus, the developed numerical algorithm allows the simulation of the entire process of the meteorite impact in a unified manner.

7 CONCLUSION

A numerical method to construct three-dimensional adaptive moving meshes has been developed. It has been implemented for solving the non-stationary three-dimensional Euler equations for compressible flows with strong moving shock waves. The approach does not require any interpolation of the solution from one mesh onto another one. The method can be extended to the Navier–Stokes equations without any substantial modification.

The developed approach has been applied to the study of the hypersonic Tunguska meteorite impact. The penetration of the meteorite into the atmosphere has been modelled from the entrance and up to the interaction with the Earth surface using a unified algorithm. The long-term evolution of the bow shock wave and the gas in the wake has also been studied. It has been shown that the meteorite substance cannot reach the Earth atmosphere. The results of the fallen tree area are in a reasonably good agreement with the observation data.

REFERENCES

1 **Thompson, J. F., Warsi, Z. U. A.,** and **Mastin, C. W.** *Numerical grid generation: foundation and applications*, 1985 (Elsevier Science Publishing, North Holland).

2 **Brackbill, J. U.** An adaptive grid with directional control. *J. Comput. Phys.*, 1993, **108**, 38–50.

3 **Azarenok, B. N.** and **Ivanenko, S. A.** Application of adaptive grids in numerical analysis of time-dependent problems in gas dynamics. *J. Comput. Math. Math. Phys.*, 2000, **40**, 1330–1349.

4 **Azarenok, B. N., Ivanenko, S. A.,** and **Tang, T.** Adaptive mesh distribution method based on Godunov's scheme. *Commun. Math. Sci.*, 2003, **1**, 152–179.

5 **Ren, W.** and **Wang, X. P.** An iterative grid redistribution method for singular problems in multiple dimensions. *J. Comput. Phys.*, 2000, **159**, 246–273.

6 **Tang, H.-Z.** and **Tang, T.** Adaptive mesh methods for one- and two-dimensional hyperbolic conservation laws. *SIAM J. Numer. Anal.*, 2003, **41**, 487–515.

7 **Anderson, D. A.** Adaptive mesh schemes based on grid speeds. AIAA paper, 1983, pp. 311–318.

8 **Budd, C. J., Huang, W.,** and **Russel, R. D.** Moving mesh methods for problems with blow-up. *SIAM J. Sci. Comput.*, 1996, **17**, 305–327.

9 **Li, S.** and **Petzold, L.** Moving mesh method with unwinding schemes for time-dependent PDEs. *J. Comput. Phys.*, 1997, **131**, 368–377.

10 **Huang, W.** and **Russell, R. D.** Analysis of moving mesh partial differential equations with spatial smoothing. *SIAM J. Sci. Comput.*, 1999, **20**, 998–1015.

11 **Huang, W.** Practical aspects of formulation and solution of moving mesh partial differential equations. *J. Comput. Phys.*, 2001, **171**, 753–775.

12 **Tang, T., Xue, W. M.,** and **Zhang, P. W.** Analysis of moving mesh methods on geometrical variables. *J. Comput. Math.*, 2001, **19**, 41–54.

13 **Beckett, G., Mackenzie, J. A., Ramage, A.,** and **Sloan, D. M.** Computational solution of two-dimensional unsteady PDEs using moving mesh methods. *J. Comput. Phys.*, 2002, **167**, 478–495.

14 **Gan'zha, D. Kh., Muzafarov, I. F.,** and **Utyuzhnikov, S. V.** The use of moving adaptive grids in algorithms with compact approximations. *J. Comput. Math. Math. Phys.*, 1995, **35**(8), 949–957.

15 **Rudenko, D. V.** and **Utyuzhnikov, S. V.** Use of dynamically adaptive grids for modeling three-dimensional unsteady gas flows with high gradients. *J. Comput. Math. Math. Phys.*, 2002, **42**(3), 377–390.

16 **Ben-Menahem, A.** Source parameters of the Siberian explosion of June 30, 1908, from analysis and synthesis of seismic signals at four stations. *Phys. Earth Planet. Inter.*, 1975, **11**, 1–35.

17 **Korobeinikov, V. P., Gusev, S. B., Chushkin, P. I.,** and **Shurshalov, L. V.** Flight and fracture of the Tunguska cosmic body into the Earth's atmosphere. *Comput. Fluids*, 1992, **21**, 323–330.

18 **Ivanov, A. G.** and **Ryzhanskii, V. A.** Possible nature of the explosion of the Tunguska meteorite and the breakup of the comet Shoemaker–Levy. *J. Combust. Explo. Shock Waves*, 1995, **31**(6), 715–721.

19 **Svetsov, V. V., Nemchinov, I. V.,** and **Teterev, A. V.** Disintegration of large meteoroids in Earth's atmosphere: theoretical models. *Icarus*, 1995, **116**, 131–153.

20 **Svetsov, V. V.** Where have the debris of the Tunguska meteoroid gone?. *Sol. Syst. Res.*, 1996, **30**(5), 378–390.

21 **Korobeinikov, V. P., Shurshalov, L. V., Vlasov, V. I.,** and **Semenov, I. V.** Complex modelling of the Tunguska catastrophe. *Planet. Space Sci.*, 1998, **46**(2/3), 231–244.

22 **Sekanina, Z.** Evidence for asteroidal origin of the Tunguska object. *Planet. Space Sci.*, 1998, **46**(2/3), 191–204.

23 **Bronshten, V. A.** The nature of the Tunguska meteorite. *Meteorit. Planet. Sci.*, 1999, **34**, 723–728.

24 **Bronshten, V. A.** Nature and destruction of the Tunguska cosmical body. *Planet. Space Sci.*, 2000, **48**, 855–870.

25 **Tirskiy, G. A.** and **Khanukaeva, D. Yu.** The modeling of bolide thermal explosions. *Earth Moon Planets*, 2004, **95**, 513–520.

26 **van Leer, B.** On the relation between the upwind-differencing schemes of Godunov, Engquist–Osher and Roe. *SIAM J. Sci. Stat. Comput.*, 1984, **5**(1), 1–20.

27 **Rodionov, A. V.** A second order monotone scheme to calculate nonequilibrium flows by shock-capturing technique. *J. Comput. Math. Math. Phys.*, 1987, **27**, 585–593.

28 **Kolgan, V. P.** Application of the minimum-derivative principle in the construction of finite-difference schemes for numerical analysis of discontinuous solutions in gas dynamics (in Russian). *Uch. Zap. TsaGI*, 1972, **3**(6), 68–77.

29 **Brackbill, J. U.** and **Saltzman, J. S.** Adaptive zoning for singular problems in two dimensions. *J. Comput. Phys.*, 1982, **46**, 342–368.

30 **Grigoryan, S. S.** On motion and destruction of meteors in planetary atmospheres. *Cosmic Res.*, 1979, **17**(2), 724–740.

31 **Utyuzhnikov, S. V., Konyukhov, A. V., Kondaurov, V. I.,** and **Mesheryakov, M. V.** Gas dynamical model of interaction between a meteorite and the Earth atmosphere. In the 2nd IAA International Conference on Low-cost Planetary Missions, 1996, pp. IAA-L-1–IAA-L-6.

32 **Hills, J. G.** and **Goda, M. P.** The fragmentation of small asteroids in the atmosphere. *Astron. J.*, 1993, **105**(3), 1114–1144.

33 **Klumov, B. A., Kondaurov, V. I., Konyukhov, A. V., Medvedev, Yu. D., Sokolskii, A. G., Utyuzhnikov, S. V.,** and **Fortov, V. E.** Collision of comet Shoemaker–Levy 9 with Jupiter: what shall we see? *J. Phys. Usp.*, 1994, **164**(6), 577–589.

34 **Utyuzhnikov, S. V.** Numerical modelling combustion of fuel-droplet-vapor releases in atmosphere. *Int. J. Flow, Turbul. Combust.*, 2002, **68**(2), 137–152.